Article

Journal of
Nanoscience and Nanotechnology
Vol. 14, 1–6, 2014
www.aspbs.com/jnn

Field Emission from Zinc Oxide Nanobelts

A. Asthana[1,*], Y. K. Yap[2], and R. S. Yassar[3,*]

[1] Department of Materials Science and Engineering, Michigan Technological University, Houghton, 49931, MI, USA
[2] Department of Physics, Michigan Technological University, Houghton, 49931, MI, USA
[3] Department of Mechanical Engineering-Engineering Mechanics, Michigan Technological University, Houghton, 49931, MI, USA

We report here, the *in-situ* field emission (FE) property measurement on the individual ZnO nanobelts inside a high resolution transmission electron microscope (TEM) using a special scanning tunneling microscopy (STM)-TEM system. The field emission properties were found to be size scale dependent. It was found that the threshold voltage decreases and the field enhancement factor increases with the decrease in the diameter of the tip of the nanobelt and increase in the sharpness of the tip. The field emission parameter was estimated following the Fowler–Nordheim (*F–N*) theory. The ZnO nanobelt with the sharp agave like tip structure ($d = 10$ nm) showed the highest value of the field enhancement factor, $\beta \approx 4562$, and a high field emission current of ~ 502 μA.

Keywords: *In-Situ* Microscopy, ZnO Nanobelt, Field Emission.

1. INTRODUCTION

Field emission (FE) is one of the many applications of one-dimensional nanostructured (1D) materials including nanotubes, nanowires, and nanorods. It is of great commercial interest in vacuum microelectronic devices such as field emission displays, X-ray sources, microwave devices, etc. As 1D materials, carbon nanotubes (CNTs) have been investigated for field emission for years. Comprehensive theoretical and experimental research on FE has been mainly conducted on CNTs owing to their good conductivity, chemical stability as well as cost effective fabrication.[1,2] An array of densely packed CNTs greatly reduces the field enhancement factor at the CNT tip to a level not much different from a flat metal plate. The loosely distributed CNT's cannot meet the desired requirement of the high current density and high emitting points. Oxide semiconducting nanostructure, which are more stable at high temperatures in an oxygen environment and exhibit a more controllable electronic property have been considered more and more as an alternative FE sources instead of CNT's. With a large exciton binding energy, thermal stability, oxidation resistant and favorable aspect ratio, ZnO nanostructures (nanowire/nanobelt/nanotube etc.) have recently been studied as an effective FE source.[3–6] ZnO nanowires/nanobelts are of interest for field emission applications particularly in flat panel displays as they can be synthesized in a well aligned and densely packed arrays. Until now, most of the studies on the field emission of ZnO nanowire/nanobelt have been carried out in a simple vacuum chamber consisting of cathode and anode and a field emission detection system.[7–10] From the extensive FE studies on the CNT's, it has been observed that field enhancement properties depend on the inter-electrode distance, radius, geometry and shape of the nanotube and the emission process is highly sensitive to the exact tip structure (open/closed end of the nanowire/nanotube).[3,5,11–13] However, it is difficult to estimate the distance precisely inside a vacuum testing chamber without microscopy attachments. In order to perform an accurate investigation, it will be highly desirable to do the *in-situ* FE experiment inside an electron microscope. There are few reports on the *in-situ* FE measurement of ZnO nanowire/nanobelt inside the scanning electron microscope (SEM), in which the emitting distance could be directly observed.[14] By *in-situ* experiment in SEM, although we can observe shape, size and geometry of the nanowire/nanotube, but it is difficult to get a clear high-resolution image of the tip structure. In comparison to this, the *in situ* FE measurement inside TEM could be a convenient and powerful method to accurately determine the FE properties with precise inter-electrode distance along with real time imaging of the shape, size and structure of the tip of the nanowire during the FE measurement.

*Authors to whom correspondence should be addressed.

In view of this, we report here, the FE property measurement on the individual ZnO nanobelts inside a high resolution TEM (JEM 4000FX, operated at 200 kV) using a special scanning tunneling microscopy (STM)-TEM holder system.

2. EXPERIMENTAL DETAILS

The *in situ* field emission experiment was conducted in a high resolution transmission electron microscope (TEM, JEM 4000FX, operated at 200 kV) using a special scanning tunneling microscopy (STM)-TEM holder system from "Nanofactory Instruments." The STM-TEM system provides a unique combination of transmission electron microscopy and scanning tunneling microscopy techniques, which are used simultaneously in one instrument for full sample characterization.[15–17] It consists of a STM equipped TEM sample holder, a controller and a PC with Nanofactory's data acquisition software. All the measurements were carried out on a single tilt STM-TEM holder in a JEM 4000FX TEM, operated at 200 kV. The electrochemically etched gold wire with ZnO nanobelt was attached to the piezo-driven movable part of the holder facing the fixed and sharp tungsten STM tip as its counter electrode, and oriented perpendicular to the electron beam in the TEM. In such an arrangement, atomic scale imaging and I–V measurements were carried out concurrently. The contact was made between the STM tip and the ZnO nanobelt by the precision movement of the gold wire (with the sample) attached to the piezo-driven manipulator. Field emission measurement was conducted by applying different bias voltages to the gold electrode with the nanobelt sample at its tip, while the tungsten STM tip was grounded. The ZnO nanobelt used in our study are grown in a double quartz tube configuration thermal Chemical Vapor Deposition (CVD) system as reported previously but without the use of Au catalyst.[18] The growth was performed in a horizontal furnace consisting of a quartz tube vacuum chamber. A closed end smaller quartz tube (60 cm long and 2 cm in diameter) containing the precursor materials and the substrates was inserted within the vacuum chamber. A mixture of ZnO (0.2 g) and graphite (0.1 g) powder in an alumina boat was used as the precursor materials. The boat is placed at the closed end of the smaller quartz tube. The temperature of the furnace was raised to 1100 °C. The substrates are in a temperature zone of ∼650 to 450 °C. The temperature was held at 1100 °C for 30 minutes and turned off to allow cooling to 600–700 °C in ∼1 hour. Experiment is stopped by switching off the furnace and allowing the system to cool down to room temperature.

3. RESULTS AND DISCUSSION

The nanobelts have width ranging from 20 to 100 nm and length of ∼2 μm. A low magnification bright field image of a nanobelt and its corresponding electron diffraction pattern (in the inset) is shown in Figure 1(a). The diffraction pattern and the corresponding high resolution image, (Fig. 1(b)) taken from the rectangular region in Figure 1(a) suggest that the ZnO nanobelt are single crystals with wurtzite hexagonal structure ($a = 0.32$ nm, $c = 0.52$ nm, P63mc), and a general growth direction of [0001].

To ensure a reliable electrical contact, it is important that nanobelts be firmly attached to the tip of the gold wire (250 μm diameter) mounted on the piezotube of the *in-situ* holder. To ensure this, the nanobelts were glued to the gold substrate by conducting silver paste. It is also important that the STM tip (i.e., W-tip) be cleaned of any oxide layer to have a better electrical contact with the nanobelt. To ensure this, the side of the gold tip (without any sample) was moved into contact with the STM tip. The sharp W tip was readily melted on passing a large current through the tips, resulting in a clean W tip with slightly larger radius. The cleaned STM tip was brought in contact with the ZnO nanobelt by moving the gold wire (with the sample attached) connected with the piezo driven tube. After this, the nanobelt was again moved to touch the counter electrode, the sharp W tip with a bias of 10 V and a current

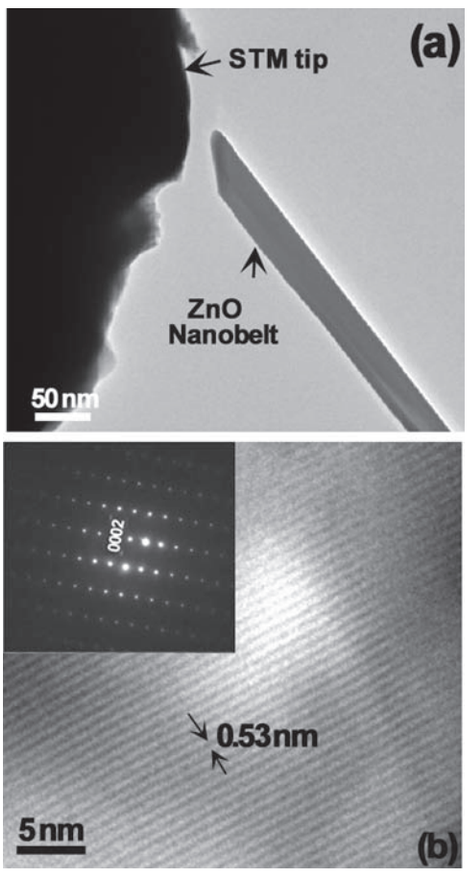

Figure 1. (a) A ZnO nanobelt and its (b) corresponding electron diffraction pattern (inset) and the high-resolution lattice image.

limited of 1 mA. The nanotube was observed to be slightly melted at the tip and the total resistance of the nanobelt was also reduced to several tens of kΩ by current annealing and then it is pulled back by moving the piezo driven tube leaving a fresh ZnO nanobelt surface at the tip. The nanobelt was then retracted to a suitable place in between the two electrodes for field emission measurement.

Several nanobelts with different shapes and dimensions were investigated for field emission properties. Field emission measurements were conducted by applying different bias voltages to the gold electrode with the nanobelt sample at its tip, while the tungsten STM tip was grounded. A maximum of 140 V was applied between the nanobelt and the counter W tip and typically the acquisition time for each field emission I–V curve with 1000 data points was 5000 ms. Every field emission current voltage (I–V) curve is an average of typically 10–20 I–V sweep cycles.

Figures 2(a)–(f) show the bright field images of ZnO nanobelts with different tip geometries aligned between the two counter electrodes during the field emission process. These nanobelts can be categorized into nanobelts with width, $w = 10$–200 nm on the top and width of 100–300 nm at the bottom, and nanobelts with uniform width.

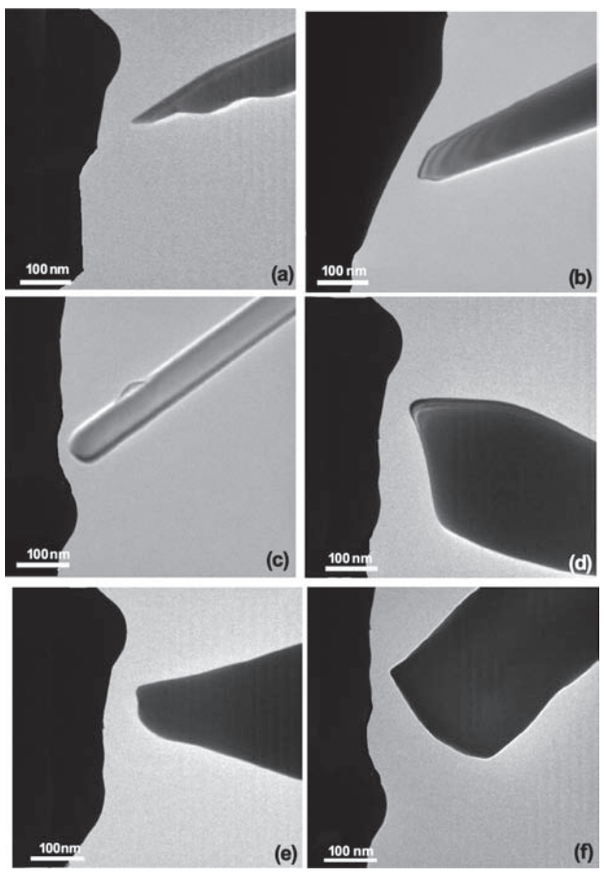

Figure 2. The bright field images of the ZnO nanobelts with different tip shape and width, w ranging from 10–200 nm.

Figures 3(a) depicts typical field emission current (I) obtained from various nanobelts shown in Figures 2(a)–(c). For I–V curves in the low voltage region, the emitted current is very low and seems to be independent of the applied field. It is observed that both threshold voltage and the field emission current depend on the shape and tip diameter of the nanobelt. The threshold voltage for the emission current was low (∼6.50 V and 8.05 V, Fig. 3(a)) for the nanobelt having sharp agave like tip structure (Figs. 2(a) and (b), width, $w = 10$ nm and 18 nm) as compared to the nanobelt having a round tip ($w = 22$ nm, Figs. 2(c), 3(a)). The threshold voltage for the round-tip nanobelt is ∼15.04 V (curve "c", Fig. 3(a)). The I–V curves for the broader-tip nanobelts (Figs. 2(d)–(f)) ($w = 40$ nm, 80 nm and 200 nm) are shown in Figure 3(b). There is a sharp increase of field emission current with the voltage, once the threshold voltage is reached to start the electron emission. Once the emission is fully operating, I–V follows the Fowler–Nordheim emission.[19] The highest emission current of ∼502.5 μA is obtained for the sharp agave like tip nanobelt (Fig. 2(a), $w = 10$ nm) with low turn-on voltage of 6.75 V. This is followed by emission current of ∼425.6 μA for nanobelt also having sharp agave like tip structure, $w = 18$ nm at turn-on voltage of ∼8.75 V. For the round-shaped tip nanobelt, the field emission current was ∼190.54 μA, with turn-on voltage of ∼15.04 V. As is evident (Fig. 4(b)), with the increase in the width and decrease in the sharpness of the tip, the threshold voltage increases and field emission current decreases. The field emission current was found to be ∼216 μA ($w = 40$ nm, turn-on field ∼20.86 V), 112.35 μA ($w = 80$ nm, turn-on voltage ∼40.88 V) and 40 μA ($w = 200$ nm, turn-on voltage ∼77.4 V). It is to be noted that the agave like-tip nanobelt and higher diameter of 40 nm produces the field emission current of nearly ∼216 μA, which is higher than the field emission current (I) from that of obtained by the round-shaped tip of width, $w = 22$ nm ($I \sim 190.54$ μA). This indicates that geometrical shape of the tip affects the field emission properties. Yang et al. also found that the geometry of the micro- and nanostructural emitters play a crucial role in the field emission of ZnO.[20]

The emission current–voltage characteristics were analyzed by using the Fowler–Nordheim (F–N) theory. According to the F–N theory the field emission current density is

$$J = a(\beta^2 V^2/\phi d^2)\exp[-bd\phi^{3/2}/\beta V]$$

where J is current density, a and b are universal constants given by $a = 1.5414 \times 10^{-6}$ AeVV^{-2} and $b = 6.830888 \times 10^9$ eV$^{-3/2}$ Vm^{-1},[19] and ϕ is the work function of the ZnO. The local electric field E is related to the potential difference between the ZnO nanobelt tip and the counter electrode via $E = \beta V/d$, β being a local field conversion factor and d is the inter-electrode distance. Assuming $I = JA$, with A being the emission area, we obtain

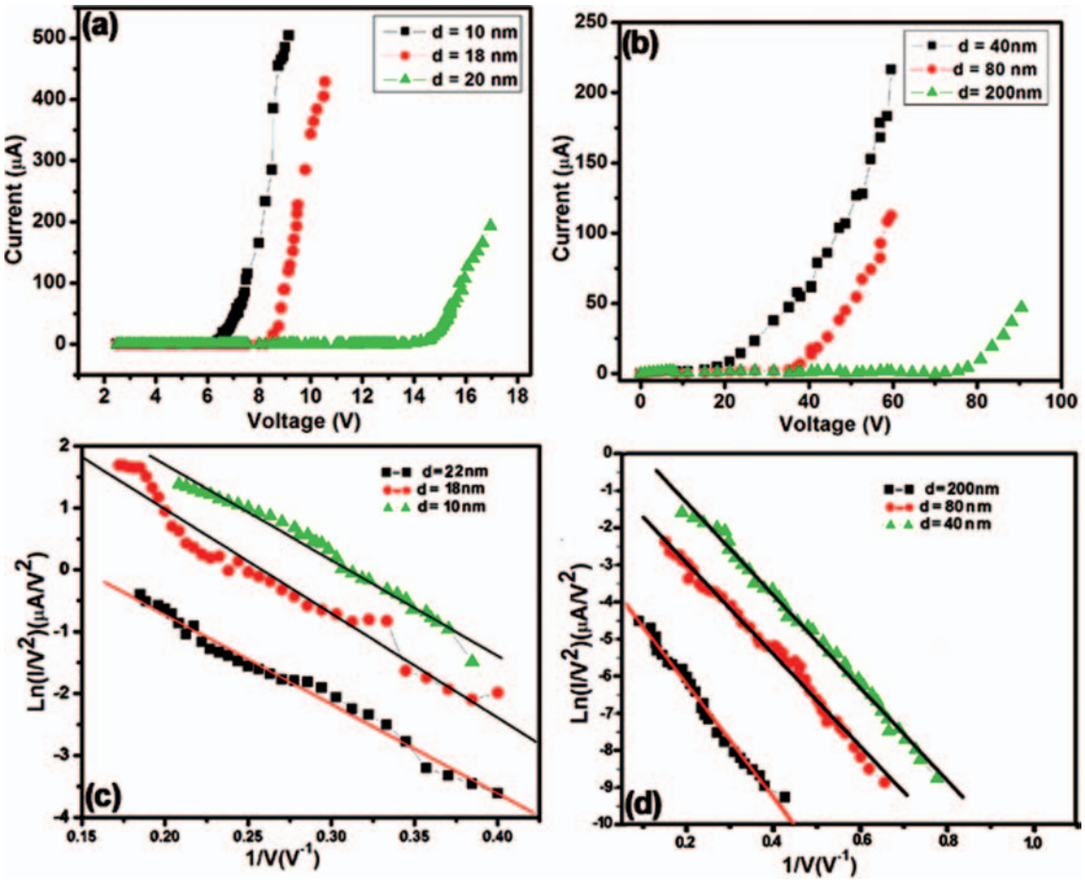

Figure 3. (a) The I–V curves of the nanobelts having width, $w \sim 10$, 18 and 22 nm. (b) I–V curves of the nanobelts having $w \sim 40$, 80 and 200 nm. (c) The F–N plots of the nanobelts having $w \sim 10$, 18 and 22 nm and (d) The F–N plots of the nanobelts having $w \sim 40$, 80 and 200 nm.

$$\ln(I/V^2) = \ln(Aa\beta^2 V^2/\phi d^2) - bd\phi^{3/2}/\beta V \qquad (1)$$

To determine the field enhancement factor β, it is easy to trace the F–N plot through $\ln(I/V^2)$ versus $1/V$, which follows a linear relationship with the slope dependence of ϕ and β. The enhancement factor, β can thus be determined by fitting the slope value and taking a reasonable ϕ value. Figure 4(c) depicts the F–N plots of nanobelts with agave like tip ($w = 10$ nm), ($w = 18$ nm), and roundlike-tip ($w = 22$ nm) showing that the field emission behavior of the nanobelts was in agreement with the F–N theory. This indicated that the emission was governed by the electron tunneling from the top layer at the very end of the ZnO nanobelts. The slope of the linear correlation is given by $B\phi^{3/2}d/\beta$ with $B = 6.87 \times 10^9$ (Ve $V^{-3/2}$ m^{-1}). The work function of ZnO was assumed to be 5.4 eV. From the slope of the F–N plot (Fig. 3(c)), the estimated field enhancement factor, β for the nanobelts ($w = 10$ nm and 18 nm) are 4562 and 3255 and for the round tip nanobelt, the β is estimated to be 2435. For the nanobelts with broader tip width ($w = 40$ nm, 80 nm and 200 nm), the estimated β values from the F–N plots (Fig. 3(d)) are 2840, 2532 and 315 which are in agreement with the reported results from ZnO nanowires/nanobelts.[20–26] As was observed, the estimated field enhancement factor, β decreases with the increase in the tip diameter and broader shape of the tip of the nanobelts. The variation of field enhancement factor, β with the tip diameter of the nanobelts is shown in Figure 4.

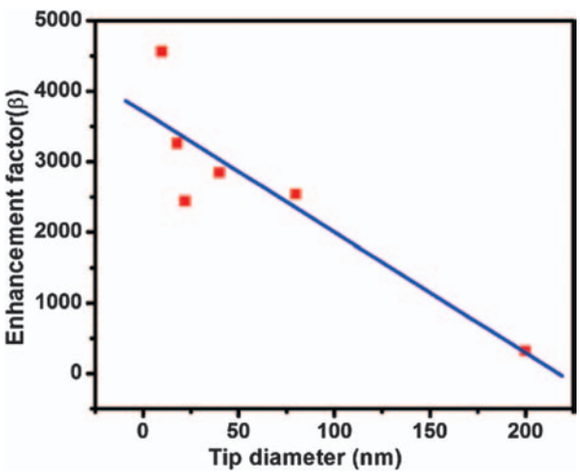

Figure 4. The variation of field enhancement factor, β with the tip diameter of the nanobelts.

Table I. A comparison of the field emission parameters of ZnO nanobelts (NB) having different tip diameter and shapes.

Width, d (nm)	Tip shape	Turn on voltage (V)	Field emission current (μA)	Field enhancement factor, β
10	Agave like	6.75	502.5	4562
18	Agave like	8.75	425.6	3255
22	Round	15.04	190.54	2435
40	Agave like	20.86	216	2840
80	Agave like	40.88	112.35	2532
200	Round	77.4	40	315

A comparison of the various field emission parameters of ZnO nanobelts (NB) having different tip diameter and shapes is given in Table I.

Based on the above experimental results, the geometrical factor of the nanostructure plays a crucial role in their field emission ability. Ku et al. demonstrated that the tip cone angle (θ) and the tip radius (R_{tip}) are two important factors for the field emission.[27] Both θ and R of the agave like tip of the nanobelt is the smallest among the other nanobelt tips shown schematically in Figure 5. This indicates that the field emission of the agave like structure seems to be the best among all the structure. One of the factors for the better field emission in agave like tip structure as compared to the round tip structure of similar diameter is the size of the emitting area. The emitting area of the agave like structure including the tip and side area of the cone is larger than that of round tip structure, which has only small side area and only the top surface of the tip contributes for the field emission. Other factor is the pointed shape of the tip with smaller diameter in agave like structure as compared to round tip and flat tip with larger diameter. As it is known that field-assisted emission depends exponentially on the field via Eq. (1), it can be enhanced by shaping the cathode (i.e., tip of the nanobelt in the present study) into a cone with a sharp point where the field is maximum and the electron emission occurs from the tip. Hence, it is understandable that agave like structure will act as a better field emitter than the round and flat tips. One of the other factor for the

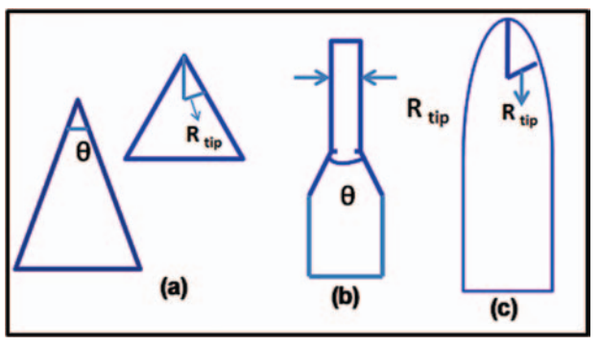

Figure 5. Schematic diagram presenting the shape of the tip of the nanobelts (a) agave like (b) pencil like (c) round structure.

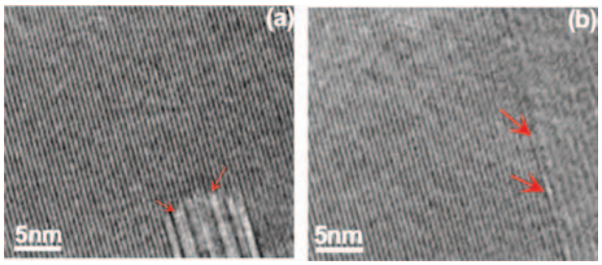

Figure 6. HRTEM image of the tip of the nanobelt. The planar defects in the image are marked by red arrow.

low threshold field for the field emission current and large value of the enhancement factor, β for the nanobelt shown in Figures 2(a), (b) can be the presence of defect at the tip. A careful structural examination shows the presence of planar defects like stacking faults and also some point defects (shown in Figs. 6(a), (b), marked by red arrow) in the region near the tip. These defects can alter the electronic structure by producing the localized resonant states that result in band gap reduction and hence can reduce the threshold voltage required for the field emission.[28–31]

In the present investigations, the effect of electron beam was minimized by conducting the structural characterization at a low beam current of 2.91 nA. The manipulation of the nanowires was done at a much lower beam current of 0.72 nA. The low beam current of 0.72 nA and 2.91 nA was obtained by adjusting the possible combination of condenser aperture and spot size. The electron beam was spread to avoid any convergence of the beam on the sample. In addition, we shut off the electron beam while recording force–displacement data. Thus the related contamination and electron beam induced structural damage is decently minimized. Recent theoretical calculations show that the local temperature is no more than a few degrees above the room temperature under low beam currents.[32] In some of our previous works[15–17, 33, 34] the low current beam radiation did not induce any detectable change in the conductivity of the nanowires indicating that the effect of electron beam can be ignored in the analysis of the data presented in this work.

4. CONCLUSIONS

In conclusion, it can be said that the field emission measurement of the individual ZnO nanobelts have been carried out *in-situ* inside a high resolution TEM. It was observed that both threshold voltage and the field emission current depend on the shape and tip diameter of the nanobelt. There is a decrease in the threshold voltage to start the field emission and increase in the value of the field enhancement factor, β as the diameter of the ZnO nanowire decreases. The nanobelt having agave like tip structure and smaller diameter (10 nm) tip was found to be the best field emitter under the present investigations. The highest field emission current of $\sim$502.5 μA and largest

value of field enhancement factor, β (= 4562) are obtained for the above nanobelt.

Acknowledgment: The authors would like to acknowledge the funding support through the NSF-DMR grant No. 0820884 and NSF-CMMI grant No. 0926819.

References and Notes

1. W. A. de Heer, A. Chatelain, and D. Ugarte, *Science* 270, 1197 (**1995**).
2. S. Fan, M. G. Chapline, N. R. Franklin, T. W. Tombler, A. M. Cassell, and H. Dai, *Science* 283, 512 (**1999**).
3. C. J. Lee, T. J. Lee, S. C. Lyu, Y. Zhang, H. Ruth, and H. J. Lee, *Appl. Phys. Lett.* 81, 3648 (**2002**).
4. Y. W. Zhu, H. Z. Zhang, X. C. Sun, S. O. Feng, J. Xu, Q. Zhao, B. Xiang, R. M. Wang, and D. P. Yu, *Appl. Phys. Lett* 83, 144 (**2003**).
5. S. H. Jo, J. Y. Lao, Z. F. Ren, R. A. Farrer, T. Baldacchini, and J. T. Fourkas, *Appl. Phys. Lett.* 83, 4821 (**2003**).
6. H. S. Nalwa, (eds.), Encyclopedia of Nanoscience and Nanotechnology, American Scientific Publishers, Los Angeles, CA (**2004/2011**), Vols. 1–25.
7. Y. H. Yang, B. Wang, N. S. Xu, and G. W. Yang, *Appl. Phys. Lett.* 89, 043108 (**2006**).
8. J. Xu, G. Hou, B. Dong, Y. Chang, Y. Wang, H. Yan, and B. Yu, *Nanosci. Nanotechnol. Lett.* 5, 1081 (**2013**).
9. Z. Shi, T. Ding, J. Wu, and C. Xu, *Nanosci. Nanotechnol. Lett.* 5, 267 (**2013**).
10. L. C. Ying, L. S. Yi, L. Pang, and T. T. Yuen, *J. Nanosci. Nanotechnol.* 5, 1088 (**2005**).
11. L. F. Dong, J. Jiao, D. F. Tuggle, J. M. Petty, S. A. Elliff, and M. Coulter, *Appl. Phys. Lett.* 81, 3648 (**2002**).
12. S. H. Jo, D. Banerjee, and Z. F. Ren, *Appl. Phys. Lett.* 85, 1407 (**2004**).
13. Y. H. Wang, C. X. Wang, B. Wang, N. S. Xu, and G. W. Yang, *Chem. Phys. Lett.* 403, 248 (**2005**).
14. X. Wang, J. Zhou, C. Lao, J. Song, N. Xu, and Z. L.Wang, *Adv. Mater.* 19, 1627 (**2007**).
15. A. Asthana, T. Shokuhfar, Q. Gao, P. Heiden, C. Friedrich, and R. S. Yassar, *Appl. Phys. Lett* 97, 1 (**2010**).
16. A. Asthana, T. Shokuhfar, Q. Gao, P. A. Heiden, C. Friedrich, and R. S. Yassar, *Adv. Sci. Lett,* 3, 557 (**2010**).
17. A. Asthana, K. Momeni, A. Prasad, Y. K. Yap, and R. S. Yassar, *Applied Physics: A* 105, 909 (**2011**).
18. S. L. Menshah, V. K. Kayastha, and Y. K. Yap, *J. Phys. Chem. C* 111, 16092 (**2007**).
19. R. H. Fowler and L. W. Nordheim, *Proc. R. Soc. London, Ser. A* 119, 173 (**1928**).
20. Y. H. Yang, B. Wang, N. S. Xu, and G. W. Yang, *Appl. Phys. Lett* 89, 043108 (**2006**).
21. G. Zhang, Q. Zhang, Y. Pei, and L. Chen, *Vacuum* 77, 53 (**2004**).
22. Q. H. Li, Q. Wan, Y. J. Chen, T. H. Wang, H. B. Jia, and D. P. Yu, *Appl. Phys. Lett* 85, 636 (**2004**).
23. U. K. Gautam, L. S. Panchakarla, B. Dierre, X. Fang, Y. Bando, T. Sekiguchi, A. Govindaraj, D. Goldberg, and C. N. Rao, *Adv. Funct. Mater.* 19, 131 (**2009**).
24. W. Z. Wang, B. Q. Zeng, J. Yang, B. Poudel, J. Y. Huang, M. J. Naughton, and Z. F. Ren, *Adv. Mater.* 18, 3275 (**2006**).
25. Y. B. Li, Y. Bando, and D. Goldberg, *Appl. Phys. Lett.* 84, 3603 (**2004**).
26. W. Wang, G. Zhang, L. Yu, X. Bai, Z. Zhang, and X. Zhao, *Physics E* 36, 86 (**2007**).
27. T. K. Ku, M. S. Chen, C. C. Wang, M. S. Feng, I. J. Hsieh, J. C. M. Huang, and H. C. Cheng *Jpn. J. Appl. Phys. Part I* 34, 5789 (**1995**).
28. Y. B. Li, Y. Bando, T. Sato, and K. Kurashima, *Appl. Phys. Lett.* 81, 144 (**2002**).
29. H. Y. Peng, M. D. McCluskey, Y. M. Gupta, M. A. Kneissl, and N. M. Johnson, *Phys. Rev. B* 71, 1152071 (**2005**).
30. K. Nishidate and M. Hasegawa, *Phys. Rev. B* 78, 195403 (**2008**).
31. S. D. Mahanti, K. Hoang, and S. Ahmad, *Physica B* 401, 291 (**2007**).
32. I. Jencic, M. W. Bench, I. M. Robertson, and M. A. Kirk, *J. Appl. Phys.* 78, 974 (**1995**).
33. A. Asthana, K. Momeni, A. Prasad, Y. K. Yap, and R. S. Yassar, *Applied Phys. Lett* 95, 172106 (**2009**).
34. A. Asthana, K. Momeni, A. Prasad, Y. K. Yap, and R. S. Yassar, *Nanotechnology* 22, 245101 (**2011**).

Received: 8 December 2013. Accepted: 7 January 2014.